



# Optics Letters

## Fast Raman spectral mapping of highly fluorescing samples by time-gated spectral multiplexed detection

CHRISTOPHER J. CORDEN,<sup>1</sup>  DUSTIN W. SHIPP,<sup>1</sup>  PAVEL MATOUSEK,<sup>2</sup> AND IOAN NOTINGER<sup>1,\*</sup>

<sup>1</sup>School of Physics and Astronomy, University of Nottingham, Nottingham NG7 2RD, UK

<sup>2</sup>Central Laser Facility, Research Complex at Harwell, STFC Rutherford Appleton Laboratory, UKRI, Harwell Oxford, Didcot OX11 0QX, UK

\*Corresponding author: ioan.notinger@nottingham.ac.uk

Received 11 September 2018; accepted 7 October 2018; posted 16 October 2018 (Doc. ID 335878); published 21 November 2018

**We present a time-gated Raman micro-spectroscopy technique suitable for fast Raman mapping of samples eliciting large laser-induced fluorescence backgrounds. To achieve the required time resolution for effective fluorescence rejection, a picosecond pulsed laser and a single-photon avalanche diode were used. A module consisting of a spectrometer, digital micromirror device, and two prisms was used for high-resolution spectral filtering and multiplexing, which is required for a high chemical specificity and short integration times. With this instrument, we demonstrated time-gated Raman imaging of highly fluorescent samples, achieving acquisition times as short as 3 min for 40 × 40 pixel resolution images.**

Published by The Optical Society under the terms of the [Creative Commons Attribution 4.0 License](https://creativecommons.org/licenses/by/4.0/). Further distribution of this work must maintain attribution to the author(s) and the published article's title, journal citation, and DOI.

<https://doi.org/10.1364/OL.43.005733>

Raman micro-spectroscopy is a powerful tool for mapping molecular properties of samples with diffraction-limited spatial resolution [1]. However, a major source of noise for many samples arises from laser-induced fluorescence emission, which is a concurrent phenomenon with Raman scattering. This fluorescence background signal, in some cases, can be orders of magnitude higher than the Raman signal itself. If the relatively weak Raman signal is of the same order (or smaller) as the shot noise caused by the fluorescence signal, then the Raman signal is lost.

Many techniques have been proposed over the years to counteract the effects of fluorescence emission [2–6]. Computational techniques can subtract the fluorescence background, but cannot eliminate the fundamental shot noise caused by the fluorescence photons. Using an excitation laser wavelength in the 700–830 nm near-infrared region can reduce the likelihood of fluorescence excitation for many samples in order to facilitate reasonably short integration times (0.1–1 s) required in hyperspectral Raman mapping. Nevertheless, this approach may still not be

sufficient for a range of systems such as pigmented samples (e.g., pigmented biological samples, art and archeology artefacts, geology). Operating in the time domain, while still maintaining near-infrared excitation using picosecond pulsed lasers, has proven to be one of the most effective methods for dealing with highly fluorescent samples in Raman spectroscopy. Using this approach, the Raman and fluorescence photons can be separated in the time domain, thus preventing the latter from being measured and eliminating the photon shot noise associated with fluorescence emission.

The existing time-gating Raman spectroscopy techniques use either direct optical gating or time-correlated single-photon counting. The optical gating techniques use typically an optical Kerr Gate [7] or an iCCD camera [8] and achieve high fluorescence suppression and high-spectral resolution, but can require long acquisition times. While the optical Kerr gating offers the highest temporal resolution and choice of excitation wavelength, it requires a complex system that includes powerful pulsed laser systems to activate the Kerr medium, restricting its implementation into specialist laboratories. In principle, iCCDs could provide an effective solution, but noise created by the intensifiers results in a limited signal-to-noise ratio.

Time-correlated single-photon counting techniques use a high temporal resolution detection system to record the time of arrival of each photon, and a scanning monochromator is used to record a Raman spectrum. However, Raman mapping requires a large number of measurements (e.g., 10,000 spectra for a 100 × 100 image), making mapping not practical. Multichannel single-photon avalanche diode (SPAD) arrays have been developed [9–13] that can reduce the acquisition times. However, these multichannel SPAD devices, which are still in the developmental stage, have a low fill factor, and the temporal resolution of the combined array is typically poorer than that of a single detector.

Here we present a simple time-gated Raman micro-spectroscopy technique that overcomes the above-mentioned limitations. A single SPAD element was used as a detector, as it allows for optimum temporal resolution and, thus, effective fluorescence rejection. To minimize the acquisition time for mapping, we selected a high-repetition-rate picosecond laser

(10 MHz) and a wavelength multiplexing detection system based on a spectrometer and a digital micromirror device (DMD).

DMDs have been used in conjunction with spectrometers, both for spectral [14,15] and spatial filtering [16,17] (but not in a time-gated mode); here we used two prisms to recombine the spectrally filtered Raman photons onto the single SPAD element in order to provide spectral multiplexing. While this configuration does not provide any advantage when acquiring full Raman spectra (scanning of DMD elements is still required), the high-resolution spectral filtering enabled by the DMD, combined with the spectral multiplexing, single SPAD element, and high-repetition laser enabled molecular mapping of highly fluorescent samples at high speed, while maintaining a high chemical specificity. The DMD spectral filter can be optimized for only one compound at a time, requiring a separate acquisition for each target compound.

A schematic description of the instrument is presented in Fig. 1. A 35 ps pulsed DFB diode laser with 775 nm wavelength (Katana 775, 65 mW average power, 5 nJ pulse energy, 10 MHz rep rate) was focused on the samples via an optical microscope (Nikon) equipped with a 50 $\times$  and 0.50 NA objective (Leica N PLAN L) and a translation stage (PI 542). The Raman scattered photons, together with the elastically scattered and fluorescence photons, were collected by the same objective and collimated towards a spectrometer (Andor Shamrock 303i) equipped with a 300 lines/mm grating. A long-pass filter (BLP01-785) was used to block the elastically scattered light from entering the spectrometer. The spectrometer was equipped with a deep-depletion back-illuminated CCD (DU401 Andor). By switching a mirror, it was possible to direct the dispersed Raman and fluorescence light via a side port onto a DMD (Texas Instruments DLP3000). Lenses L1 and L2 relay the image plane from the spectrometer output port onto the DMD. As each spatial element of the DMD corresponds to a specific wavelength,

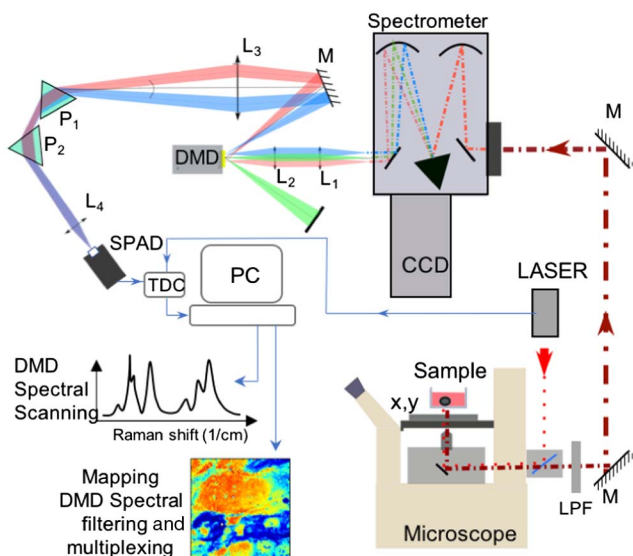


**Fig. 1.** Schematic description of the instrument (not to scale). DMD, digital micromirror device; SPAD, single-photon avalanche photodiode; TDC, time-to-digital converter; L1, L2, L3, L4, lenses; P1, P2, prisms; M, mirror; LPF, 780 nm long-pass filter; x, y, microscope translation stage.

the DMD can be used for high-resolution spectral filtering. The light corresponding to the selected wavelengths is recombined via two equilateral prisms and then focused by lens L4 onto a 50  $\mu\text{m} \times 50 \mu\text{m}$  area SPAD (MPD 50CT SPAD). The prisms were selected to obtain the desired amount of dispersion, and lens L3 was selected to match the dispersion angles from the spectrometer to the dispersion of the prisms, such that the entire selected wavelength range was successfully recombined to form a collimated polychromatic beam. The arrival of each pulse from the SPAD was compared with the Katana laser sync pulse via a time-to-digital converter (TDC) with 10 ps temporal resolution (TDC GPX2 by ams). A microcontroller handled the configuration of the TDC and the data acquisition via SPI communication, which then sent the photon detection data in binary serial format to a personal computer. The instrument time response was approximately 190 ps, which is currently limited by the SPAD used.

Figure 2 compares spectra of non-fluorescing materials (e.g., polystyrene [PS]) acquired using the conventional Raman setup based on the CCD with spectra of the same samples acquired by scanning the DMD elements sequentially (referred to as “DMD scanning”). (The spectral range of 650–1650  $\text{cm}^{-1}$  and resolution of 10  $\text{cm}^{-1}$  were kept the same.) Only minor differences related to the relative intensity of the bands were observed; these were attributed to the differences in the

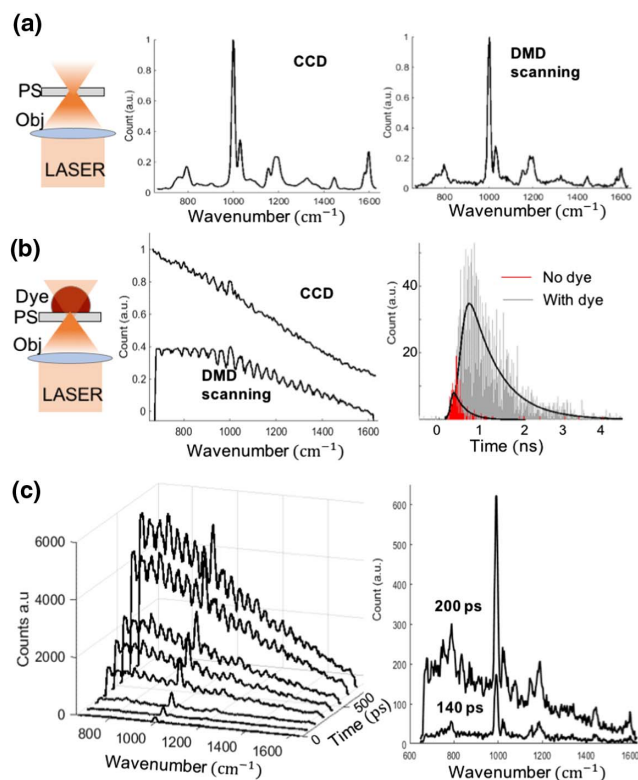


**Fig. 2.** (a) Comparison between the Raman spectra of a PS sample acquired with the conventional CCD and with the new setup in the DMD scanning mode without time-gating (all time components integrated). (b) Same as (a) but after a drop of a red 730 dye (lifetime  $\sim 1$  ns) was added on the PS. The time distribution of the detected photons before (red) and after adding the fluorescent dye (gray) is presented on the right. (c) Time-gated Raman spectra of the PS/dye acquired in the DMD scanning mode. Acquisition time: 200 s.

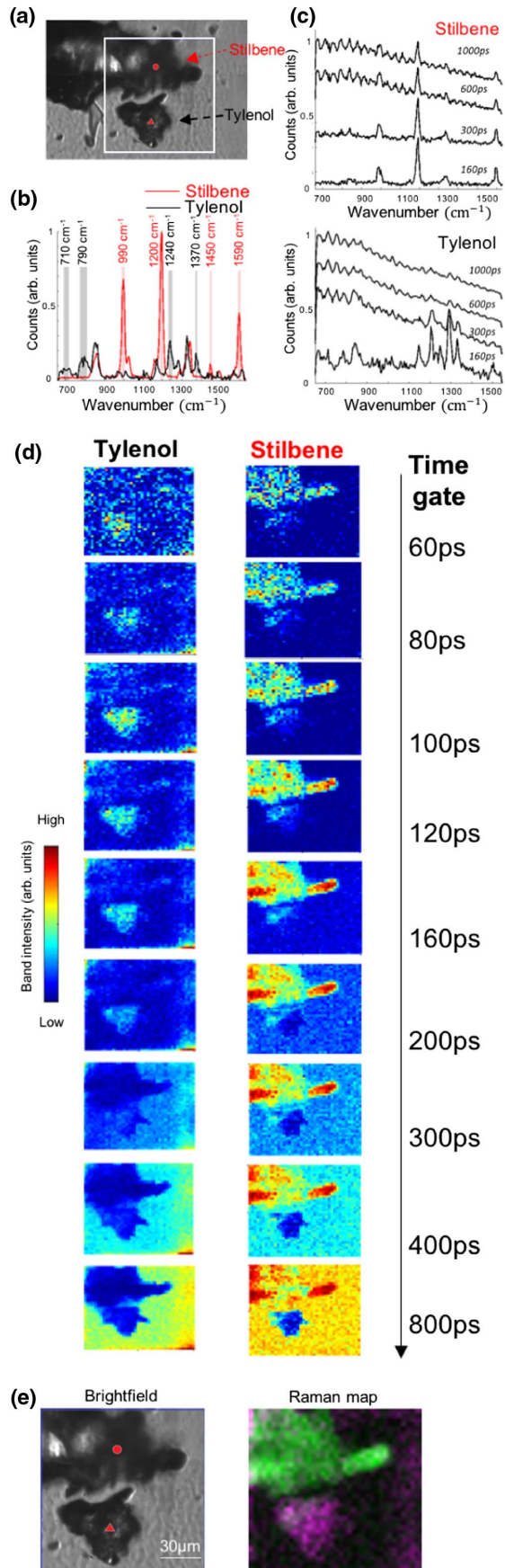


Fig. 3. (Continued)

wavelength dependence of the optical components and detection efficiency of the SPAD and CCD.

Figure 2 shows that all main bands measured in the conventional Raman spectrum of PS acquired with the CCD can be identified in the spectrum measured in the DMD scanning mode.

To evaluate the ability of the instrument to discriminate between Raman and fluorescence photons (i.e., fluorescence rejection), the experiments were repeated after adding a highly fluorescent dye (Sigma Aldrich fluorescent red 730 78581—lifetime  $\sim 1$  ns, maximum absorption/emission wavelengths: 680 and 755 nm, respectively) solution on top of the PS sample. Figure 2(b) shows that the Raman bands of PS are swamped by the broad fluorescence background, both for the spectrum acquired with the CCD and the spectrum acquired in the DMD scanning mode without time-gating. The main band of the PS at  $1004\text{ cm}^{-1}$  corresponding to the ring breathing mode can hardly be distinguished. Nevertheless, the histograms of the timing of photon detection events [Fig. 2(b)] show that the Raman bands could be recovered effectively by time-gating the detection. The time-gated Raman spectra of the PS/dye sample [Fig. 2(c)] show that, for time gates shorter than 200 ps, the Raman bands of the PS can be observed clearly. [The bands in the spectra acquired at 140 ps are similar to those in Fig. 2(a).] The level of fluorescence suppression depends on the time gate and the characteristics of the electronic transition responsible for the fluorescence emission.

While the results in Fig. 2 demonstrate efficient rejection of the fluorescence photons, the new detection scheme in a DMD scanning mode, however, presents no specific advantages compared to previously reported time-gated Raman spectroscopy using single SPAD elements and scanning monochromators. The advantage of the DMD scheme becomes evident when operating the instrument in a “DMD spectral multiplexing” mode, which allows simultaneous detection of the Raman photons corresponding to selected Raman bands of interest, with high-spectral resolution filtering ( $10\text{ cm}^{-1}$  for this instrument) and high-efficiency rejection of the fluorescence photons. The acquisition of a higher number of Raman photons, at a high repetition rate offered by the laser (10 MHz), leads to significantly shorter integration times and makes time-gated Raman spectral mapping practical.

To demonstrate these advantages, we selected a sample consisting of trans-stilbene and Tylenol (paracetamol) powder on a glass coverslip, covered by a small amount of fluorescent dye solution [Fig. 3(a)]. The time-gated Raman spectra of Tylenol and stilbene measured in the DMD scanning mode before adding the fluorescence were used to identify the Raman bands that provide the highest spectral discrimination between the two materials [Fig. 3(b)]. The spectral features were then

Fig. 3. (a) Bright-field image of the Tylenol (paracetamol) and stilbene powder on a glass coverslip (mapping area  $120\text{ }\mu\text{m} \times 120\text{ }\mu\text{m}$ ). (b) Time-gated spectra of stilbene (circle) and Tylenol (triangle). The bands used for multiplexing are highlighted. (c) Time-gated Raman spectra for multiplexing at the same locations after the addition of the fluorescing dye on top of the sample. (d) Time-gated Raman maps acquired in the DMD multiplexing mode corresponding to the Tylenol (left) and stilbene (right) bands. Acquisition times: 3 min for stilbene maps, 27 min for the Tylenol maps. (e) Combined pseudo-color Raman map: Tylenol (purple) and stilbene (green); the time gate was 120 ps for Tylenol and 160 ps for stilbene; total time, 30 min.

carefully chosen to maximize the Raman signal while minimizing the spectral overlap. In the example presented here, the bands unique to Tylenol were selected at 710, 790, 1240, and 1370  $\text{cm}^{-1}$  [highlighted in gray in Fig. 3(b)], while the bands unique to stilbene were the 990, 1200, 1450, and 1590  $\text{cm}^{-1}$  [highlighted in pink in Fig. 3(b)]. After adding the fluorescent dye, time-gated Raman spectra were collected at the same locations [Fig. 3(c)].

The results show that the Tylenol bands can be efficiently recovered for time gates as long as 160 ps, but they become covered by the fluorescence background at time gates longer than 300 ps. A similar increase in the fluorescence background at longer time gates is observed for stilbene; however, stilbene molecules have a higher Raman scattering cross section, and some bands can be identified, even for time gates as long as 1000 ps.

After identification of the specific bands for Tylenol and stilbene, time-gated Raman maps were acquired by raster scanning the sample through the laser focus over an area of 120  $\mu\text{m} \times 120 \mu\text{m}$  (3  $\mu\text{m}$  step size, corresponding to 40  $\times$  40 pixels) [Fig. 3(d)]. To obtain the time-gated Raman maps of Tylenol, the DMD elements corresponding to the 710, 790, 1240, and 1370  $\text{cm}^{-1}$  were selected to reflect the Raman photons towards the SPAD, while all other DMD elements were switched to reflect the light corresponding to all other wavelengths towards the beam block. For the Raman maps highlighting the areas of stilbene, only the DMD elements corresponding to the 990, 1200, 1450, and 1590  $\text{cm}^{-1}$  were turned towards the SPD. This spectral multiplexing allowed the acquisition of the time-gated Raman signals with integration times of 1 s per pixel for Tylenol and 0.1 s per pixel for stilbene. The total measurement times for the 40  $\times$  40 pixel resolution images were 27 min for the Tylenol and 3 min for the stilbene (a total scan time for both materials of approximately 30 min). To obtain the time-gated Raman maps, the raw data from the scans were separated into 20 ps bins and the resulting images are shown in Fig. 3(d) (no further processing applied). The gate width that provides the greatest signal-to-noise ratio depends on the optical properties of the sample, the Raman intensity, and the lifetime and intensity of the fluorescence. As such, the optimum gate width varies from sample to sample. As we are operating in a time-correlated single-photon counting mode, all photons are recorded with their respective time of detection tagged, and the ideal time gate can be determined after measurement by inspection.

The time-gated Raman spectral maps show that the two materials, Tylenol and stilbene, can be distinctly identified up to time gates of 200 ps. Beyond this time, the stilbene signal increases, but the Raman photons generated by Tylenol become buried in the fluorescence background. The Tylenol images show the highest signal-to-noise ratio at a gate width of 120 ps; the stilbene sample displays an optimum contrast at 160 ps. For long time-gate values (e.g., 800 ps), the Raman photons are swamped by the fluorescence photons; the Tylenol and stilbene particles cannot be discriminated. (They appear as regions of low signals, as they block part of the fluorescence photons emitted by the dye molecules.)

Here we present a simple and practical technique for time-gated Raman spectral mapping. To overcome the main limitations of current time-gated Raman spectroscopy techniques, we utilized a high repetition pulsed near-infrared laser with a single element detector to enable high temporal resolution. Using a spectral filtering/multiplexing approach based on a spectrometer as the wavelength dispersive element, a DMD as the wavelength

selective component, and prisms to recombine the spectrum allowed the acquisition of the Raman photons with integration times as short as 0.1–1 s per pixel. Such short integration times enabled spectral mapping within practical time scales (e.g., 3–30 min) for samples for which the CW Raman bands were fully buried by the fluorescence background [Fig. 3(e)]. While here we utilized a simple multiplexing technique for proof-of-principle, the DMD can be programmed for more complex multivariate spectral measurements to maximize chemical discrimination, as previously demonstrated for conventional continuous-wave Raman spectroscopy and imaging [18,19]. In addition, the ability to acquire photons with flexible selection of the time gate allows us to optimize the time gate for each chemical component of the sample, or enable simultaneous multimodal Raman and fluorescence lifetime imaging. While our proof-of-principle experiments used standard materials commonly used in Raman spectroscopy, this is a platform technique that could be applied to a range of applications dealing with samples eliciting high fluorescence levels.

**Funding.** Engineering and Physical Sciences Research Council (EPSRC) (EP/L025620/1).

**Acknowledgment.** The authors thank Prof. Anthony Kent (University of Nottingham) for useful discussions and initial tests.

## REFERENCES

1. D. W. S. Shipp, F. S. Sinjab, and N. Notingham, *Adv. Opt. Photonics* **9**, 315 (2017).
2. P. Matousek, M. Towrie, C. Ma, W. M. Kwok, D. Phillips, W. T. Toner, and A. W. Parker, *J. Raman Spectrosc.* **32**, 983 (2001).
3. J. Kostamovaara, J. Tenhunen, M. Kögler, I. Nissinen, J. Nissinen, and P. Keränen, *Opt. Express* **21**, 31632 (2013).
4. S. Dochow, N. Bergner, C. Krafft, J. Clement, M. Mazilu, B. B. Praveen, P. C. Ashok, R. Marchington, K. Dholakia, and J. Popp, *Anal. Methods* **5**, 4608 (2013).
5. S. Burgess and I. W. Shepherd, *J. Phys. E* **10**, 617 (1977).
6. D. Wei, S. Chen, and Q. Liu, *Appl. Spectrosc. Rev.* **50**, 387 (2015).
7. P. Matousek, M. Towrie, and A. W. Parker, *Appl. Spectrosc.* **53**, 1485 (1999).
8. E. V. Efremov, J. B. Buijs, C. Gooijer, and F. Ariese, *Appl. Spectrosc.* **61**, 571 (2007).
9. J. Holma, I. Nissinen, J. Nissinen, J. Kostamovaara, and S. Member, *IEEE Trans. Instrum. Meas.* **66**, 1837 (2017).
10. D. E. Schwartz, E. Charbon, and K. L. Shepard, *IEEE J. Solid-State Circuits* **43**, 2546 (2008).
11. J. M. Pavia, M. Scandini, S. Lindner, M. Wolf, and E. Charbon, *IEEE J. Solid-State Circuits* **50**, 2406 (2015).
12. I. Nissinen, J. Nissinen, P. Keränen, D. Stoppa, and S. Member, *IEEE Sens. J.* **18**, 3789 (2018).
13. Y. Maruyama, J. Blacksberg, and E. Charbon, *IEEE J. Solid-State Circuits* **49**, 179 (2014).
14. N. T. Quyen, E. Da Silva, N. Q. Dao, and M. D. Jouan, *Appl. Spectrosc.* **62**, 273 (2008).
15. D. S. Wilcox, G. T. Buzzard, B. J. Lucier, P. Wang, and D. Ben-Amotz, *Anal. Chim. Acta* **755**, 17 (2012).
16. Z. Liao, F. Sinjab, G. Gibson, M. Padgett, and I. Notingham, *Opt. Express* **24**, 12701 (2016).
17. F. Sinjab, D. Awuah, G. Gibson, M. Padgett, A. M. Ghaemmaghami, and I. Notingham, *Opt. Express* **26**, 25211 (2018).
18. C. Scotté, H. B. de Aguiar, D. Marguet, E. M. Green, P. Bouzy, S. Vergnole, C. P. Winlove, N. Stone, and H. Rigneault, *Anal. Chem.* **90**, 7197 (2018).
19. O. G. Rehrauer, V. C. Dinh, B. R. Mankani, G. T. Buzzard, B. J. Lucier, and D. Ben-Amotz, *Appl. Spectrosc.* **72**, 69 (2018).